Bone 67 (2014) 193–199

Contents lists available at ScienceDirect

Bone

journal homepage: www.elsevier.com/locate/bone

Original Full Length Article

Human Proximal Femur Bone Adaptation to Variations in Hip Geometry

M.M. Machado [a], P.R. Fernandes [a,*], V. Zymbal [b], F. Baptista [b]

[a] LAETA, IDMEC, Instituto Superior Técnico, Universidade de Lisboa, Av. Rovisco Pais, 1 1049-001 Lisboa, Portugal
[b] CIPER, Faculdade de Motricidade Humana, Universidade de Lisboa, Estrada da Costa, 1499-002, Cruz Quebrada, Dafundo, Portugal

ARTICLE INFO

Article history:
Received 20 December 2013
Revised 30 June 2014
Accepted 1 July 2014
Available online 9 July 2014

Edited by: Sundeep Khosla

Keywords:
hip geometry
proximal femur
biomechanics
bone adaptation
bone mineral density

ABSTRACT

The study of bone mass distribution at proximal femur may contribute to understand the role of hip geometry on hip fracture risk. We examined how bone mineral density (BMD) of proximal femur adapts to inter individual variations in the femoral neck length (FNL), femoral neck width (FNW) and neck shaft angle (NSA). A parameterized and dimensionally scalable 3-D finite element model of a reference proximal femur geometry was incrementally adjusted to adopt physiological ranges at FNL (3.90-6.90 cm), FNW (2.90-3.46 cm), and NSA (109-141°), yielding a set of femora with different geometries. The bone mass distribution for each femur was obtained with a suitable bone remodelling model. The BMDs at the integral femoral neck (FN) and at the intertrochanteric (ITR) region, as well as the BMD ratio of inferomedial to superolateral (IM:SL) regions of FN and BMD ratio of FN:ITR were used to represent bone mass distribution. Results revealed that longer FNLs present greater BMD (g/cm^3) at the FN, mainly at the SL region, and at the ITR region. Wider FNs were associated with reduced BMD at the FN, particularly at the SL region, and at the ITR region. Larger NSAs up to 129° were associated with BMD diminutions at the FN and ITR regions and with increases of the IM:SL BMD ratio while NSAs larger than 129° resulted in decrease of the IM:SL BMD ratio. These findings suggest hip geometry as moderator of the mechanical loading influence on bone mass distribution at proximal femur with higher FNL favoring the BMD of FN and ITR regions and greater FNW and NSA having the opposite effect. Augmented values of FNL and FNW seem also to favor more the BMD at the superolateral than at the inferomedial FN region.

Introduction

Hip fracture is an important public health and personal burden which is anticipated to continue to rise due to increased life span [1,2]. The ability of bone to resist fracture depends on its material composition (i.e., amount and properties of the materials that form the bone) and the spatial distribution of the bone mass [3]. Moreover, it is well established that the risk of fracture is multi-factorial and many independent risk factors have been identified to enhance the specificity and sensitivity of predictive fracture risk models [1,2,4]. Despite the suggestion of hip geometry as risk factor for hip fracture [5–9], no consensus has been achieved so far about which geometric parameters improve the prediction of fracture risk. The inconsistency among studies of femoral geometry and hip fracture can be attributed to several factors, including study design (retrospective vs prospective), variability in measurement techniques, sample size limitations and the fact that most studies have combined all the types of hip fracture (femoral neck - cervical, trochanteric or intertrochanteric fractures) [10]. Currently, even the most complex fracture risk prediction tools do not integrate hip geometric characteristics as risk factors in clinical practice [4].

A reasonable approach to link hip geometry and hip fracture may be to analyze first if isolated variations in certain proximal femur geometric parameters give rise to particular spatial bone mass distribution patterns, especially as it has been shown that bone mass distribution at the proximal femur is associated with hip fracture risk [3,11]. Thus, with the objective of testing if similar mechanical load generates different effects on bone mass distribution at the proximal femur according to the hip geometry, this study proposes to map, by means of a three-dimensional finite element method and a pre-validated bone remodeling model, the distribution of bone mass at the proximal femur and examine its association with the geometric parameters that are commonly assessed, namely the femoral neck length (FNL), the femoral neck width (FNW) and the neck-shaft angle (NSA).

Material and Methods

Development of a parameterized 3-D finite element model (FEM)

The left proximal femur geometry of the adult 'Standardized Femur' 3-D model [12], derived from a CT-scan dataset of a composite human femur replica, was discretized using tetrahedral elements, giving rise to a refined and uniform size mesh (207502 elements, 39285 nodes,

* Corresponding author. Fax: +351 218417915.
E-mail addresses: miguelmm.machado@gmail.com (M.M. Machado), prfernan@dem.ist.utl.pt (P.R. Fernandes), verazymbal@fmh.ulisboa.pt (V. Zymbal), fbaptista@fmh.ulisboa.pt (F. Baptista).

http://dx.doi.org/10.1016/j.bone.2014.07.001
8756-3282/

Abaqus FEA® element type C3D4, 4-node linear element, average edge-length of 2 mm, Joe-Liu mesh quality metric (0-1) [13] of 0.85) (Fig. 1 A). The type and number of elements were decided in order to minimize the error on stress and strain evaluation (convergence study) and, at the same time, to have a good resolution on the bone apparent density distribution which is computed assuming bone density is constant within each element. The Cartesian coordinates of the nodes forming the finite element mesh were imported to Matlab R2013a (8.1.0.604) as a point cloud, from which the following measures were calculated according to Mahaisavariya et al. [14]: femoral head centre; neck isthmus centre; femoral neck axis; femoral shaft axis; intersection of the femoral neck axis and the proximal shaft axis; FNL; FNW and NSA (Fig. 1 B). Three geometric parameters frequently assessed at the proximal femur were investigated: FNL, FNW (measured at the narrowest part of femoral neck) and NSA [10]. The parameterized model geometry was scaled by applying an affine transformation to the nodes within the finite element mesh belonging to the proximal femur region R (Fig. 1 B). The inter-distance of the mesh nodes not belonging to that region were not changed [6]. Sixteen individual finite element models (FEMs) were created based on the reference FEM to represent the three geometric features and their physiological variances in the human population: six FEMs for FNLs and five FEMs per each of the remaining geometric features (Fig. 1 C).

Finite element modeling: boundary conditions

The procedure to define the boundary conditions consisted of an adaptation of the musculoskeletal model and derived load profiles developed and validated by Bergmann [15] and Heller et al. [16,17], from which hip contact and muscle forces and the position of their acting points were taken. The muscle system included the abductors (*gluteus minimus*, *gluteus maximus*, *gluteus medius* and *tensor fascia latae*) and the. *vastus lateralis* (Fig. 1 A). Due to anatomical differences between the available musculoskeletal model and the used finite element model, a manual procedure was used to match the position of the acting points defined in the musculoskeletal model with the element surfaces of the reference finite element geometry.

A load case corresponding to the instant of peak hip contact force observed in the stance phase of a "typical" gait cycle was used (Table 1).

In order to generate a physiological loading condition, the forces applied to each individual surface element of the FEM's were not concentrated at the attachment locations but distributed over neighboring surfaces [18]. Thus, muscles forces were uniformly distributed over elements surface based on previously measured physiological muscle attachment areas [19]. Regarding hip contact force, a physiological hip contact surface area was also considered [20], in which the load decreases linearly with the distance from the acting point to zero on the edge of the highlighted area (Fig. 1 A). The general surface traction – Dsload *Abaqus 6.9* feature was used to define loads in a user-defined non-normal surface direction. The components of the traction vector load were calculated given the force vectors presented in Table 1 and the area of the elements surface.

The femoral bone was constrained in the mid-diaphysis to suppress rigid body motion. Since we intended to study the femur bone adaptation in different femur geometries, it was important to determine whether changes in the studied geometric parameters influence hip loading, which consequently would influence bone strains and thus bone remodeling [21,22]. Indeed, estimates of hip loading have been shown to be sensitive to femoral geometric features [24,25]. Of particular interest in this work are the observations of Lenaerts et al. [26] who found that increased femoral neck length resulted in increased peak hip

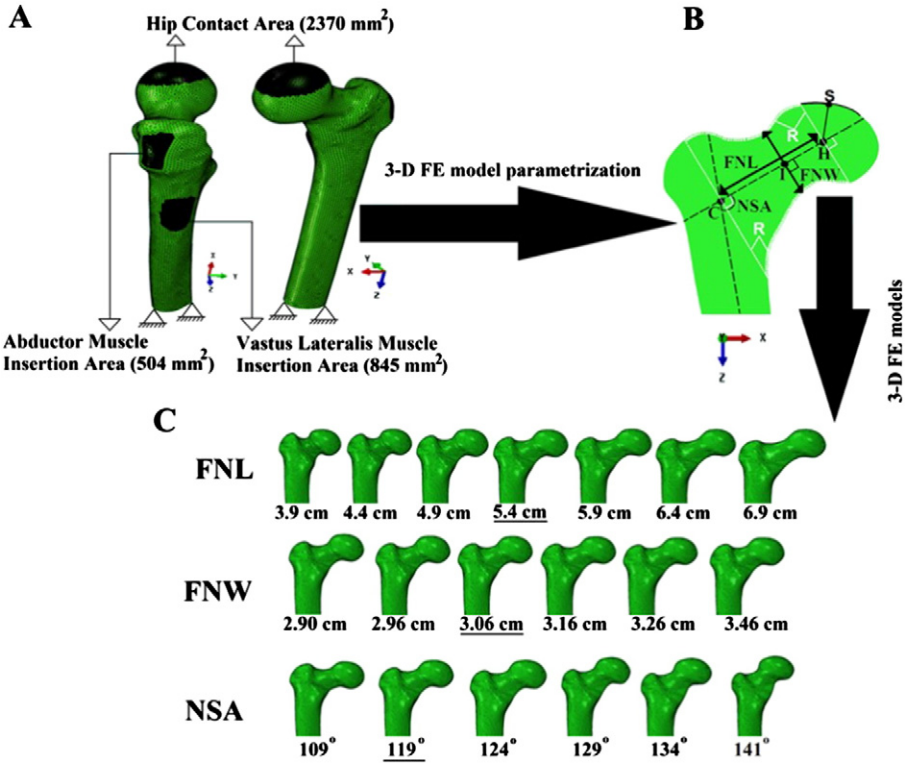

Fig. 1. Finite element model approach: A) Three dimensional (3-D) finite element model of the reference proximal femur. The areas highlighted in black represent the surfaces of application of the muscle and contact forces. The axis + z and + x is directed downwards and medially, respectively, while the axis + y is directed posteriorly. B) Schematic representation of geometric parameters: H – femoral head centre; I – neck isthmus centre; S - center of the femoral head surface; H-S – hip contact force direction; H-I – femoral neck axis; C - intersection of the femoral neck axis with the proximal shaft axis; FNL – femoral neck length; FNW – femoral neck width; NSA – neck shaft angle; R – proximal femur region wherein inter-distance of mesh nodes were changed. C) Whole set of finite element models separated by geometric characteristics. The underlined models represent the reference model for the corresponding feature.

Table 1
Loading environment at the proximal femur during single leg stance.

Activity cycle	Subject-specific geometry	Force type	F_x,F_y,F_z %BW
Gait	All geometries	F_h	-52.7279, 32.4336, 224.2159
		F_a	64.9845, -15.2670, -81.0495
		$F_{v.l}$	-0.9025, -18.4965, 92.9005
	Longer FNL models	F_{h^*}	F_h + (-89.2, 50.8, 94.2) %BW/cm
		F_{a^*}	F_a - (0.619, -0.145, -0.772)×35 %BW/cm
		$F_{v.l^*}$	$F_{v.l}$

FNL-femoral neck length; F_h–hip contact force; F_a– abductor muscle force; F_a– *vastus lateralis* muscle force; F_*– forces adjusted for subject-specific FNL geometry; Fx, Fy and Fz - components of force in the x, y and z directions (coordinate system shown in Fig. 2); BW – body weight (it was considered a body mass of 836 Newton, according to Heller et al. [17]).
* – Loading adjustment for the femoral longer neck models (FNL > 5.4 cm).

contact force and reduced vertical orientation of the loading during single leg stance, while an altered femoral NSA had only a minor effect on the loading configuration at the hip. Therefore, in the present study no changes were performed in the NSA models regarding hip loading whereas the reference load profile was adjusted for longer FNL models (finite element models where the FNL parameter was increased regarding the reference geometry, i.e., models with FNL > 5.4 cm) by reducing the magnitude of the muscle forces 35% BW/cm while maintaining its direction (a magnitude change up to half the reference magnitude of the abductor muscle force, 52.5% BW) and by increasing the magnitude of the hip contact force vector and changing its orientation to a less vertical loading condition (Table 1). Moreover, it was assumed that FNW do not influence hip loading due to hip mechanics.

Bone remodeling model and bone material properties

A computational bone remodeling model was used in order to obtain the bone mass distribution for each femur. Here it is adopted a bone remodeling model based on the one developed by Fernandes et al. [27]. In this model bone is modeled as an orthotropic, porous, continuous and oriented material, obtained by the periodic repetition of a unit-cell with rectangular holes with dimensions $\mathbf{a} = (a_1, a_2, a_3)$ and an orientation defined by the Euler angles $\boldsymbol{\theta} = (\theta_1, \theta_2, \theta_3)$. The hole dimensions are normalized to the dimensions of the unit-cell and the relative bone density $\rho \in [0, 1]$, at each unit-cell, depends on local hole dimensions $\mathbf{a}$, i.e., $\rho = 1 - a_1 a_2 a_3$. Both $\mathbf{a}$ and $\boldsymbol{\theta}$ evolve in order to satisfy a remodeling law derived assuming that bone self-adapts in order to achieve the stiffest structure for the supported loads, and given by:

$$\sum_{r=1}^{P}\left(\alpha^r \frac{\partial E^H_{ijkl}}{\partial \boldsymbol{a}} e_{kl}(\boldsymbol{u}^r) e_{ij}(\boldsymbol{u}^r)\right) - k\frac{\partial \rho^m}{\partial \boldsymbol{a}} = \boldsymbol{0} \quad (1)$$

$$\sum_{r=1}^{P}\left(\alpha^r \frac{\partial E^H_{ijkl}}{\partial \boldsymbol{\theta}} e_{kl}(\boldsymbol{u}^r) e_{ij}(\boldsymbol{u}^r)\right) = \boldsymbol{0} \quad (2)$$

Eqs. (1) and (2) are the optimal conditions obtained by the maximization of the global bone stiffness and correspond to the bone remodeling law in the sense that whenever they are satisfied no remodeling will occur (remodeling equilibrium). These equations define the unit-cell parameters characterizing the bone density and orientation at each point, or in a bone discretized by finite elements, at each finite element where the unit-cell parameters are assumed constant. Although in this study only a single load environment was considered (Table 1), the remodeling law (1-2) assumes that bone adaptation depends on the set of loads each individual supports during his daily activities: walking, climbing stairs, siting, running, jumping, etc. Each load leads to a displacement, strain and stress field. Thus, in Eqs. (1) and (2) $\boldsymbol{u}^r$ is the set of displacement field at equilibrium calculated by finite element analyses, P is the total number of applied load cases, α^r are the load weight factors of the multiple load formulation (which are related to the frequency of occurrence of the different loads and satisfy $\sum_{r=1}^{P} \alpha^r = 1$). E^H_{ijkl} represents the homogenized bone material properties [27], e_{ij} are the components of the strain field and k and m are model parameters which introduce the inter-individual biological variability. Indeed, even for similar loading environment the remodeling response differs from individual to individual. The parameter k corresponds to the metabolic cost of bone apposition and it is of major importance since it strongly influences the total bone mass [28]. The parameter m ($m \geq 1$) also influences the total bone mass, but its main role is to control the BMD distribution. Higher values for parameter m lead to a poorer reproduction of the extreme values of the bone density range ($\rho = 0$ and $\rho = 1$) and so, the most part of finite elements tend to converge to an intermediate density [29]. In the present paper, these model parameters were calculated in order to produce physiological BMD distribution based on a previous methodology [22] and were fixed in all the computational simulations ensuring that different bone mass distribution patterns were only due to different femur geometries and thus that the qualitative results of this study were independent of these parameters. The equivalent homogenized properties are computed considering the base material to be linear elastic, with a Young's modulus of 20 GPa and a Poisson's ratio of 0.3 [31].

It should be noted that the bone remodeling model presented above has been applied with success to study the behavior of bone with respect to the mechanical loads [22,29,30,32–35]. Moreover, in the work of Santos et al. [29], a validation of the model was carried out through a quantitative comparison of the computational results with an extensive database of dual energy X-ray absorptiometry (DXA) exams. The results evidenced the predictive ability of the computational model in the estimation of femoral neck BMD.

Mapping of the bone mass distribution at the proximal femur

A selective choice of elements from the FEMs to represent each of the four regions of interest (ROIs), namely the integral femoral neck (FN), the superolateral (SL), and inferomedial (IM) femoral neck regions, and the intertrochanteric (ITR) region were processed (Fig. 2). Ward's area (W), the region of FN with the lowest BMD was disregarded due to its variable location [36].

The absolute BMD values (g/cm^3) were computed for the whole set of finite elements (calculated from the relative density values by multiplying it by a factor of 2 [37]), and sequentially for the four regions of interest considered in this work. The FN:ITR and IM:SL BMD ratios were computed from the whole set of FEMs.

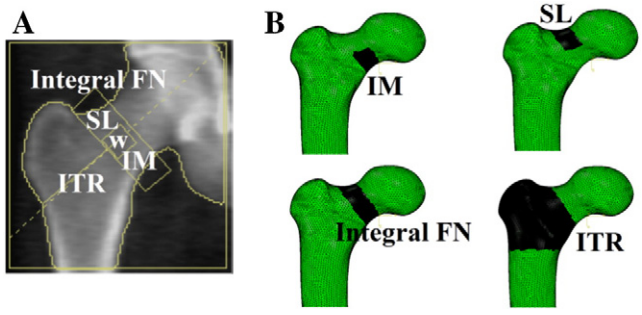

Fig. 2. Bone regions of interest at left proximal femur depicted by a DXA scan (A) and the reference computational model (B). FN – femoral neck; SL – superolateral; IM – inferomedial; ITR – intertrochanteric; W – Ward's area.

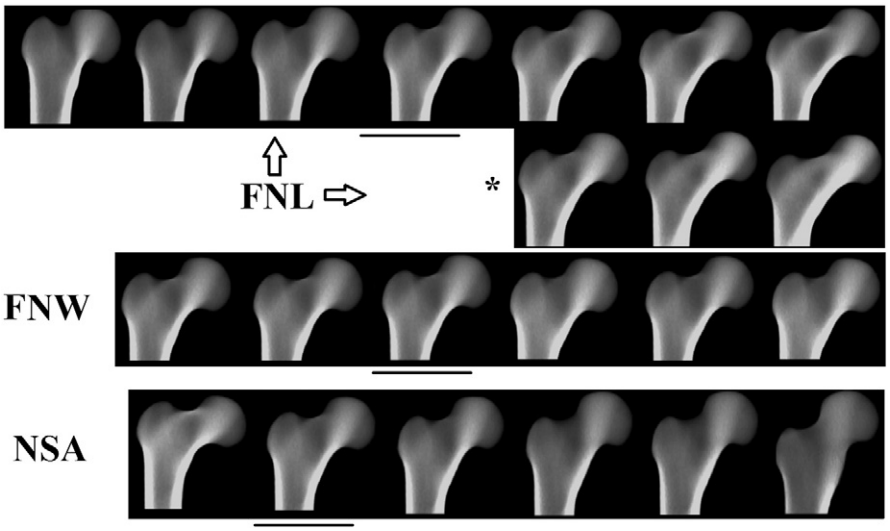

Fig. 3. Simulated proximal femur DXA images by computational analysis of finite element models according variations in the femoral neck length (FNL), femoral neck width (FNW), and neck-shaft angle (NSA). * – Loading adjustment to FNL changes.

An in-house algorithm was developed [38] to project the 3-D results of the remodeling simulations onto 2-D DXA results in order to visualize qualitatively the computational results.

Results

The predicted proximal femur bone mass distribution in the form of DXA images for the whole set of proximal femur geometries is depicted in Fig. 3.

The evolution of the BMD (g/cm^3) at the FN and ITR regions as function of FNL, FNW and NSA is graphically represented in Fig. 4. It was observed that FNL associated positively with BMD at FN and ITR regions while FNW and NSA associated negatively with BMD at these regions. The slope and the correlation coefficients for the least square linear regression models for FN and ITR bone regions between geometric parameters and BMD is presented in Table 2. Increases in the FNL from 3.9 to 6.9 resulted in an augmentation of the the FN and ITR BMD at a rate of 0.0179 gcm^{-4} and 0.0251 gcm^{-4}, respectively (increases of 0.0179 gcm^{-3} and 0.0251 gcm^{-3}, respectively per each cm). A higher BMD

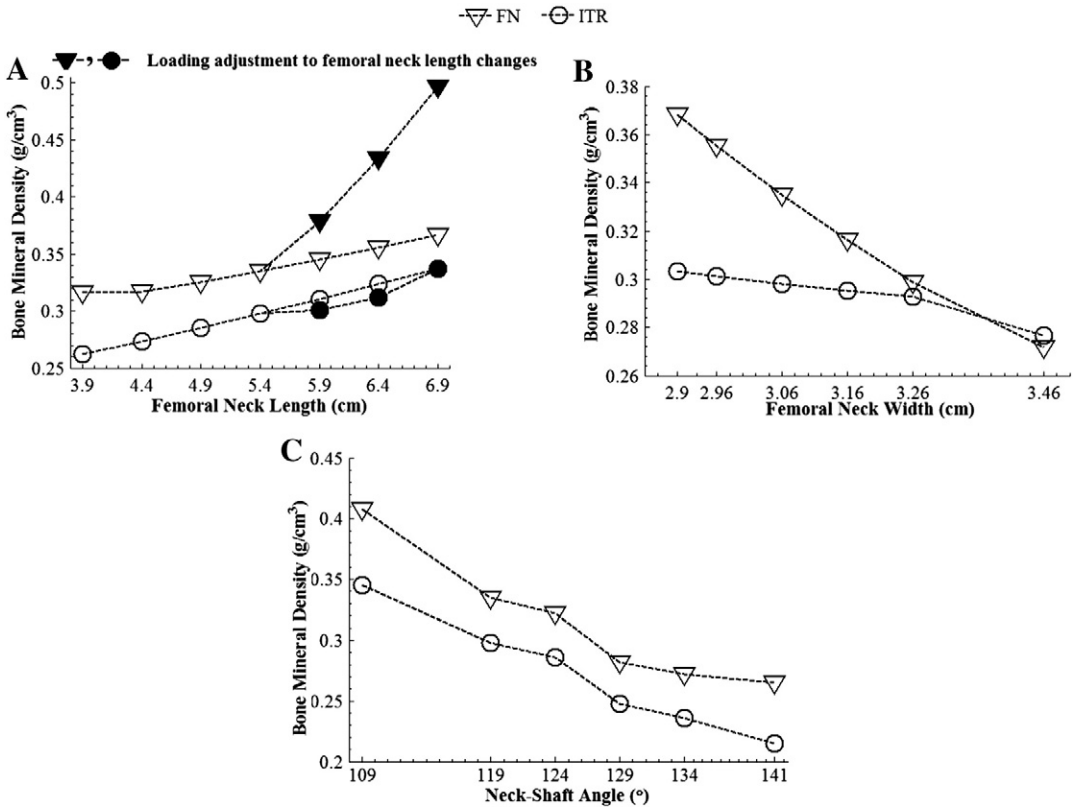

Fig. 4. Variations of bone mineral density (g/cm^3) at the femoral neck (FN) and inter trochanteric (ITR) regions of proximal femur as functions of femoral neck length (A), femoral neck width (B) and neck-shaft angle (C).

Table 2
Slope (a), ordinate at the origin (b) and correlation coefficient (r) for the least squares linear regression of bone mineral density (g/cm^3) with respect to geometric parameters of proximal femur.

Geometric parameters	Proximal femur ROI's	Linear regression parameter (a; b; r) ($BMD = a \times GP + b$)
FNL (3.9 cm–6.9 cm)	Integral FN	0.0179; 0.2408; 0.9856
	ITR	0.0251; 0.1627; 0.9997
	Integral FN *	0.1176; -0.3164; 0.9990
	ITR *	0.0261; 0.1567; 1
FNW (2.90 cm–3.46 cm)	Integral FN	-0.1732; 0.8667; -0.9956
	ITR	-0.0444; 0.4338; -0.8909
NSA (109°–141°)	Integral FN	-0.0046; 0.8900; -0.9593
	ITR	-0.0042; 0.7960; -0.9903

ROI – Regions of interest; GP – Geometric parameters; BMD – Bone mineral density; NSA – neck-shaft angle; FNL – femoral neck length; FNW – Femoral neck width; ITR – Intertrochanteric.
* – Loading adjustment for the longer femoral neck models (FNL > 5.4 cm).

increase occurred when loading adjustment was considered, mainly at the FN region, where rises in the BMD were more pronounced (rate of 0.1176 gcm^{-4} and 0.0261 gcm^{-4} for the FN and ITR regions, correspondingly). Contrary, increases in the FNW (2.90 cm – 3.46 cm) resulted in decreases of BMD at the FN and ITR at a rate of -0.1732 gcm^{-4} and -0.0444 gcm^{-4}, respectively, while increases in the NSA (109°-141°) resulted in reductions of BMD at the FN and ITR regions at a rate of -0.0046 gcm^{-3}/° and -0.0442 gcm^{-3}/°.

The behavior of the BMD ratios FN:ITR and IM:SL with respect to variations in the geometric parameters is presented in Fig. 5. Increases in the FNL resulted in a sharp decrease of the IM:SL BMD ratio and a slightly decrease of the FN:ITR BMD ratio. However, when the hip loading was adjusted to the FNL, the FN:ITR BMD ratio increased. In turn, increases in the FNW caused a decrease of the IM:SL BMD ratio and an almost unchanged behavior of the FN:ITR BMD ratio. Regarding the NSA, a non-monotonic behavior was observed for the IM:SL BMD ratio as it increased until NSA = 129° and decreased thereafter. Small changes were also observed in the FN:ITR BMD ratio.

Discussion

The main purpose of this study was to analyze proximal femur bone mass distribution at relevant bone regions and its relationships with FNL, FNW and NSA. We found that long FNL were positively associated with increased BMD at the integral FN and with low IM:SL BMD ratio, meaning a proportionally greater BMD at the superolateral region of the FN comparatively to its inferomedial region. This finding is consistent with the results presented by Voo et al. [6], who showed, for a longer FNL, a proportionally higher peak stress magnitude at the superior than at the inferior subregion of the FN. Increases in the FNL have also showed to promote bone mineral deposition at the ITR femur region. The bone mineral accrual at both regions is balanced when the load adjustment to FNL was neglected (FN:ITR BMD ratio was barely affected), but the FN:ITR BMD ratio increased sharply when the load adjustment was taken into account. This behavior is also related with the reduction of the abductor muscle force, imposed in our simulations, which was reflected in a bone mineral content decrease in their attachment areas and vicinity regions.

The enhancement of the SL region with increased FNL conjugated with either the slightly changes or the sharped increases in the FN:ITR BMD ratio for shorter and longer FNL models, respectively, suggest that a person with bigger FNL is more likely to have ITR fractures than FN (cervical) fractures. Such consideration would holds true only for healthy bones since in case of osteoporosis the structural integrity of the FN can be compromised due to the higher stress, in particular higher tensile stresses at the superior FN region that long FNs are subject to.

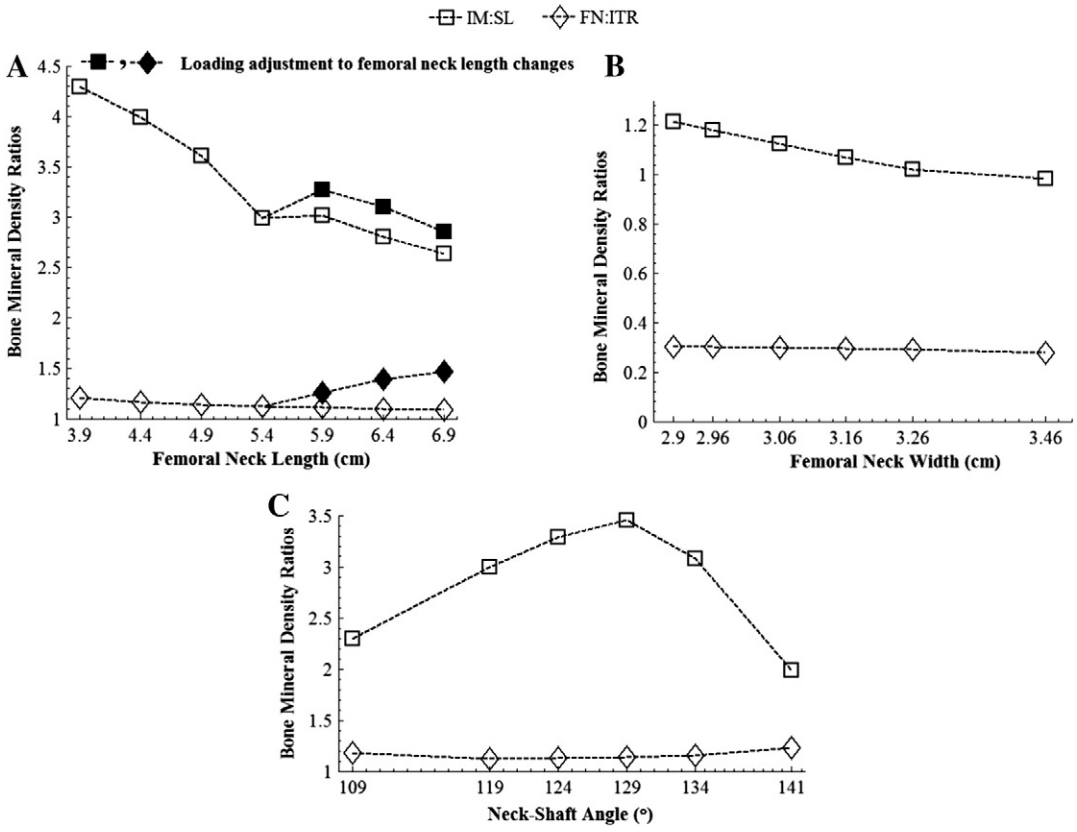

Fig. 5. Variations of IM:SL and FN:ITR BMD ratios as functions of femoral neck length (A), femoral neck width (B) and neck-shaft angle (C). FN – femoral neck; SL – superolateral; IM – inferomedial; ITR – intertrochanteric.

Fractures at the FN are more common than fractures at the ITR in women when compared to men until age 70 yrs while men are at greater risk for ITR fractures [40,41]. Such evidences can be linked with our findings if one highlight that generally men have bigger FNL than women [42], highlighting thus the importance that a balanced bone mass distribution may have in the proximal femur strength.

With respect to the FNW parameter, it was found that a femur with a wider neck presents a reduced BMD at both the FN and ITR regions when compared to a narrower neck, which can be justified by the fact that a wider FN leads to a reduced stress field within the femur structure and consequently with a generalized reduction in bone mass content. Similarly, Epelboym et al. [43] showed that robust FNs (i.e., the ones with superior FNW:FNL ratio) had a thinner and less mineralized cortical shell and a reduced trabecular BMD, a result that is corroborated by our FNW and FNL findings. By analyzing separately the superior and inferior FN regions we further verified that wider FNs present proportionally lesser BMD at the SL region of the neck comparatively to the IM region. Based on these data, we would conclude that narrow necks are stiffer than wide ones. However, the bending strength of a solid circular bar is known to be enhanced to its diameter to the forth power [10] and, as pointed out by Galileo Galilei [44], the resistance to a bone's bending (measured by section modulus) can be maintained with less material as its diameter is increased. Thus, it turns difficult to infer which situations (narrow necks with decreased IM:SL BMD ratio or wide necks with increased IM:SL BMD ratio) would more likely avoid mechanical failure beginning at the femoral neck cortex under tension. Indeed, FNW has been reported to be increased [8,9], decreased [45,46], or not different [47] when comparing subjects with and without hip fracture.

Regarding the NSA parameter our findings revealed that higher angles correlates with less bone mass at both the FN and ITR regions, a result that may be explained by a decreased stress that more vertical FNs are subject during gait. These bone mass reductions were accompanied by almost unchanged variations in the FN:ITR BMD ratio and by a decrease in the IM:SL BMD ratio with bone mass preferably added at the superior region comparatively with the inferior region of the FN for bigger NSA models (NSA > 129°) but not for small ones (NSA < 129°). The observed apparently weakness of the FN and ITR regions as NSA increases would most likely conduce to increased neck fracture risk. Indeed, epidemiological studies have consistently reported that larger NSA are associated with increased hip fracture risk [5,7].

The methodology adopted was able to analyze the effect of femoral geometric parameters as independent variables in bone adaptation, a work difficult to accomplish by any other approaches. In concrete terms, this study allowed the identification of sets of tissue-quality traits as function of hip geometry and may constitute a valuable tool to study non-invasively the stress produced on different bone geometries due to dissimilar mechanical loading, including falls [48], which is of the utmost importance since it is estimated that 90% of hip fracture result from a simple fall [2]. The FN and ITR were the selected bone regions for analyses since it correspond to locations prone to hip fracture [2] and therefore are the ones commonly assessed by DXA, the gold standard equipment for measuring BMD at the hip [39]. Beyond the absolute BMD (g/cm^3), the FN:ITR BMD ratio was also considered as an indicator of bone mass distribution since its reading offers a qualitative view on relative bone variation between fracture-critical bone regions. Moreover, because the upper neck region is also an important fracture-critical region [38], the IM:SL BMD ratio was also considered.

Biological model parameters were tuned such that the computational BMD produced at the integral FN of the reference computational model quantitatively fitted experimental reference femoral neck BMD -50th percentile of young adults [23]. Nevertheless, with the same parameters the BMD produced at the integral FN for the others FE models fell, in general, into a range of FN BMD experimentally measured [23]. It should also be noted that only one base model is tested. A different base model would likely to imply, quantitatively, different results. However, in qualitative terms it would be expected the same findings. It fact, other FE base models would fall into the range of simulated FE models for the studied geometric variables since in this study they fell into the range commonly measured in adult people. The fact that all the studied finite element models were based on a single finite element mesh (the number of finite elements and their connectivity were preserved, although the spatial coordinates of the nodes were changed) has facilitated the finite element modeling, specially the application of the boundary conditions. However, such methodology restricts the freedom in changing the nodes coordinates, since very large nodes adjustments could compromise the mesh quality. Nevertheless, this methodology showed to be suitable in simulating considerable physiological variations of proximal femur geometry without compromising the mesh quality (min vs max quality mesh: 0.83 vs 0.85). Regarding the load adjustment in the FNL models, the results should be interpreted with caution and only in a qualitative basis because muscle forces changes were inferred from muscle activation alterations by considering that both are related linearly, which is a simplification since the function that relates them is known to be complex and nonlinear [49]. Moreover, we roughly approach the Lenaerts et al. [26] muscle activation and hip contact force trends to simple linear behaviors in order to contemplate in our study the loading adjustment to FNL changes. Other limitations include the application of a single load profile which may not replicate the complex loading environment that proximal femur is submitted during activities of daily living; the assumption that muscle attachments positions and muscle cross sectional areas, as well as the area of the surfaces of application of contact forces are independent of the three studied femur geometries; the bone adaptation model assumptions. Although the change of these modeling assumptions could quantitatively influence results, the main objective of the work as well as the main conclusions would not be affected.

In summary, hip geometry showed to moderate the influence of mechanical loading in the BMD at the proximal femur producing different bone mass distribution patterns in skeletal locations where hip fractures are more common with higher FNL favoring the BMD of FN and ITR regions and greater FNW and NSA having the opposite effect. Complimentarily, increased values of FNL, FNW and NSA favored more the BMD at the superolateral than at the inferomedial FN region.

Acknowledgements

This work was funded by Portuguese Science and Technology Foundation through the project *PTDC/DES*/115607/2009.

References

[1] Metcalfe D. The pathophysiology of osteoporotic hip fracture. McGill J Med 2008;11(1):51–7.
[2] Butler M, Forte M, Kane RL, et al. Treatment of Common Hip Fractures. Evidence Report/Technology Assessments, No. 184. AHRQ Publication No. 09-E013. Rockville, M. D.: Agency for Healthcare Research and Quality; 2009
[3] Bouxsein ML. Biomechanics of Osteoporotic Fractures. Clin Rev Min Metab 2006;4(3):143–54.
[4] Johansson H, Kanis JA, Oden A, Johnell O, McCloskey E. BMD, clinical risk factors and their combination for hip fracture prevention. Osteoporos Int 2009;20(10):1675–82.
[5] Alonso CG, Curiel MD, Carranza FH, Cano RP, Pérez AD, the Multicenter Project for Research in Osteoporosis. Femoral Bone Mineral Density, Neck-Shaft Angle and Mean Femoral Neck Width as Predictors of Hip Fracture in Men and Women. Osteoporos Int 2000;11(8):714–20.
[6] Voo L, Armand M, Kleinberger M. Stress Fracture Risk Analysis of the Human Femur Based on Computational Biomechanics. Johns Hopkins Apl Tech Digest 2004;25(3):223–30.
[7] Pulkkinen P, Partanen J, Jalavaara P, Jamsa T. Combination of bone mineral density and upper femur geometry improves the prediction of hip fracture. Osteoporos Int 2004;15(4):274–80.
[8] Calis HT, Eryavuz M, Calis M. Comparison of femoral geometry among cases with and without hip fractures. Yonsei Med J 2004;45(5):901–7.
[9] El-Kaissi S, Pasco JA, Henry MJ, Panahi S, Nicholson JG, Nicholson GC, et al. Femoral neck geometry and hip fracture risk: the Geelong osteoporosis study. Osteoporos Int 2005;16(10):1299–303.
[10] Bouxsein ML, Karasik D. Bone geometry and skeletal fragility. Curr Osteoporos Rep 2006;4(2):49–56.

[11] Yang L, Burton AC, Bradburn M, Nielson CM, Orwoll ES, Eastell R, et al. Distribution of bone density in the proximal femur and its association with fracture risk in older men: The Osteoporotic Fractures in Men (MrOS) Study. J Bone Miner Res 2012;27(11):2314–24.
[12] Viceconti M, Casali M, Massari B, Cristofolini L, Bassini S, Toni A. The 'Standardized femur program' proposal for a reference geometry to be used for the creation of finite element models of the femur. J Biomech 1996;29(9):1241.
[13] Liu A, Joe B. Relationship between tetrahedron shape measures. BIT Numer Math 1994;34(2):268–87.
[14] Mahaisavariya B, Sitthiseripratip K, Tongdee T, Bohez ELJ, Sloten JV, Oris P. Morphological study of the proximal femur: a new method of geometrical assessment using 3-dimensional reverse engineering. Med Eng Phys 2002;24(9):617–22.
[15] Bergmann G. Hip98-Loading of the hip joint. Free University of Berlin3980784800; 1998 [Compact disc].
[16] Heller MO, Bergmann G, Deuretzbacher G, Dürselen L, Pohl M, Claes L, et al. Musculo-skeletal loading conditions at the hip during walking and stair climbing. J Biomech 2001;34(7):883–93.
[17] Heller MO, Bergmann G, Kassi J-P, Claes L, Haas NP, Duda GN. Determination of muscle loading at the hip joint for use in pre-clinical testing. J Biomech 2005;38(5):1155–63.
[18] Wagner DW, Divringi K, Ozcan C, Grujicic M, Pandurangan B. Combined Musculoskeletal Dynamics/Structural Finite Element Analysis of Femur Physiological Loads during Walking. Multidiscip Model Mater Struct 2010;6(4):417–37.
[19] Duda GN, Brand D, Freitag S, Lierse W, Schneider E. Variability of femoral muscle attachments. J Biomech 1996;29(9):1185–90.
[20] Genda E, Iwasaki N, Li G, MacWilliams BA, Barrance PJ, Chao EYS. Normal hip joint contact pressure distribution in single-leg standing-efect of gender and anatomic parameters. J Biomech 2001;34(7):895–905.
[21] Behrens B-A, Nolte I, Wefstaedt P, Stukenborg-Cosman C, Bouguecha A. Numerical investigations on the strain-adaptive bone remodeling in the periprosthetic femur: Influence of the boundary conditions. Biomed Eng Online 2009;8(7).
[22] Machado MM, Fernandes PR, Cardadeiro G, Baptista F. Femoral neck bone adaptation to weight-bearing physical activity by computational analysis. J Biomech 2013;46(13):2179–85.
[23] Ward KA, Ashby RL, Roberts SA, Adams JE, Mughal MZ. UK reference data for the Hologic QDR Discovery dual-energy x ray absorptiometry scanner in healthy children and young adults aged 6–17 years. Arch Dis Child 2007;92(1):53–9.
[24] Heller MO, Bergmann G, Deuretzbacher G, Claes L, Haas NP, Duda GN. Influence of femoral anteversion on proximal femoral loading: measurement and simulation in four patients. Clin Biomech 2001;16(8):644–9.
[25] Lenaerts G, Bartels W, Gelaude F, Mulier M, Spaepen A, Van der Perre G, et al. Subject-specific hip geometry and hip joint centre location affects calculated contact forces at the hip during gait. J Biomech 2009;42(9):1246–51.
[26] Lenaerts G, De Groote F, Demeulenaere B, Mulier M, Van der Perre G, Spaepen A, et al. Subject-specific hip geometry affects predicted hip joint contact forces during gait. J Biomech 2008;41(6):1243–52.
[27] Fernandes P, Rodrigues H, Jacobs C. A Model of Bone Adaptation Using a Global Optimisation Criterion Based on the Trajectorial Theory of Wolff. Comput Methods Biomech Biomed Engin 1999;2(2):125–38.
[28] Guedes J, Kikuchi N. Preprocessing and post processing for materials based on the homogenization method with adaptive finite element method. Comput Methods Appl Mech Eng 1990;83:143–98.
[29] Santos L, Romeu JC, Canhão H, Fonseca JE, Fernandes PR. A quantitative comparison of a bone remodeling model with dual-energy X-ray absorptiometry and analysis of the inter-individual biological variability of femoral neck T-score. J Biomech 2010;43(16):3150–5.
[30] Quental C, Folgado J, Fernandes P, Monteiro J. Subject-specific bone remodelling of the scapula. Comput Methods Biomech Biomed Engin 2014;17(10):1129–43.
[31] Currey J. The mechanical adaptation of bones. Princeton University Press; 1984.
[32] Fernandes PR, Folgado J, Jacob s C, Pellegrini V. A contact model with ingrowth control for bone remodelling around cementless stems. J Biomech 2002;35(2):167–76.
[33] Folgado J, Fernandes PR, Jacobs C, Pellegrini V. Influence of Femoral Stem Geometry, Material and Extent of Porous Coating on Bone Ingrowth and Atrophy in Cementless Total Hip Arthroplasty: An Iterative Finite Element Model. Comput Methods Biomech Biomed Engin 2009;12(2):135–45.
[34] Espinha L, Fernandes PR, Folgado J. Computational Analysis of Bone Remodeling during an Anterior Cervical Fusion. J Biomech 2010;43(15):2875–80.
[35] Quental C, Folgado J, Fernandes PR, Monteiro J. Bone remodelling analysis of the humerus after a shoulder arthroplasty. Med Eng Phys 2012;34(8):1132–8.
[36] Cardadeiro G, Baptista F, Zymbal V, Rodrigues LA, Sardinha LB. Ward's area location, physical activity, and body composition in 8- and 9-year-old boys and girls. J Bone Miner Res 2010;25(11):2304–12.
[37] Helgason B, Perilli E, Schileo E, Taddei F, Brynjólfsson S, Viceconti M. Mathematical relationships between bone density and mechanical properties: a literature review. Clin Biomech 2008;23(2):135–46.
[38] Tarala M, Janseen D, Verdonschot N. Balancing incompatible endoprosthetic design goals: A combined ingrowth and bone remodeling simulation. Med Eng Phys 2011;33(3):374–80.
[39] National Osteoporosis Foundation (NOF). Clinician's Guide to Prevention and Treatment of Osteoporosis. Washington, DC: National Osteoporosis Foundation; 2010.
[40] Karagas MR, Lu-Yao GL, Barrett JA, Beach ML, Baron JA. Heterogeneity of hip fracture: Age, race, sex, and geographic patterns of femoral neck and trochanteric fractures among the US elderly. Am J Epidemiol 1996;143(7):677–82.
[41] Löfman O, Berglund K, Larsson L, Toss G. Changes in hip fracture epidemiology: redistribution between ages, genders and fracture types. Osteoporos Int 2002;13(1):18–25.
[42] Traina F, Clerico M, Biondi F, Pilla F, Tassinari E, Toni A. Sex differences in Hip Morphology: Is stem Modularity Effective for Total Hip Replacement? J Bone Joint Surg 2009;91(6):121–8.
[43] Epelboym Y, Gendron RN, Mayer J, Fusco J, Nasser P, Gross G, et al. The Interindividual Variation in Femoral Neck Width Is Associated With the Acquisition of Predictable Sets of Morphological and Tissue-Quality Traits and Differential Bone Loss Patterns. J Bone Miner Res 2012;27(7):1501–10.
[44] Galilei Linceo G. Discorsi e dimonstrazioni matematiche intorno a due nuove scienze attenti alla macanica e I movimenti locali. Leiden: Elsevier; 1638.
[45] Seeman E, Duan Y, Fong C, Edmonds J. Fracture site-specific deficits in bone size and volumetric density in men with spine or hip fracture. J Bone Miner Res 2001;16(1):120–7.
[46] Karlamangla AS, Barrett-Connor E, Young J, Greendale GA. Hip fracture risk assessment using composite indices of femoral neck strength: the Rancho Bernardo study. 2004;15(1):62–70.
[47] Bergot C, Bousson V, Meunier A, Laval-Jeanet M, Laredo JD. Hip fracture risk and proximal femur geometry from DXA scans. Osteoporos Int 2002;13(7):542–50.
[48] Keyak JH, Rossi SA. Prediction of femoral fracture load using finite element models: an examination of stress- and strain-based failure theories. J Biomech 2000;33(2):209–14.
[49] Buchanan TS, Lloyd DG, Manal K, Besier TF. Neuromusculoskeletal modeling: Estimation of muscle forces and joint moments and movements from measurements of neural command. J Appl Biomech 2004;20(4):367–95.